

Archival Report

Calcium-Dependent Hyperexcitability in Human Stem Cell-Derived Rett Syndrome Neuronal Networks

Kartik S. Pradeepan, Fraser P. McCready, Wei Wei, Milad Khaki, Wenbo Zhang, Michael W. Salter, James Ellis, and Julio Martinez-Trujillo

ABSTRACT

BACKGROUND: Mutations in *MECP2* predominantly cause Rett syndrome and can be modeled in vitro using human stem cell-derived neurons. Patients with Rett syndrome have signs of cortical hyperexcitability, such as seizures. Human stem cell-derived *MECP2* null excitatory neurons have smaller soma size and reduced synaptic connectivity but are also hyperexcitable due to higher input resistance. Paradoxically, networks of *MECP2* null neurons show a decrease in the frequency of network bursts consistent with a hypoconnectivity phenotype. Here, we examine this issue.

METHODS: We reanalyzed multielectrode array data from 3 isogenic *MECP2* cell line pairs recorded over 6 weeks ($n = 144$). We used a custom burst detection algorithm to analyze network events and isolated a phenomenon that we termed reverberating super bursts (RSBs). To probe potential mechanisms of RSBs, we conducted pharmacological manipulations using bicuculline, EGTA-AM, and DMSO on 1 cell line ($n = 34$).

RESULTS: RSBs, often misidentified as single long-duration bursts, consisted of a large-amplitude initial burst followed by several high-frequency, low-amplitude minibursts. Our analysis revealed that *MECP2* null networks exhibited increased frequency of RSBs, which produced increased bursts compared with isogenic controls. Bicuculline or DMSO treatment did not affect RSBs. EGTA-AM selectively eliminated RSBs and rescued network burst dynamics.

CONCLUSIONS: During early development, *MECP2* null neurons are hyperexcitable and produce hyperexcitable networks. This may predispose them to the emergence of hypersynchronous states that potentially translate into seizures. Network hyperexcitability depends on asynchronous neurotransmitter release that is likely driven by pre-synaptic Ca^{2+} and can be rescued by EGTA-AM to restore typical network dynamics.

<https://doi.org/10.1016/j.bpsgos.2024.100290>

Mutations of the X-linked gene *MECP2*, coding for a global transcriptional regulator that is critically involved in the development of the nervous system, cause Rett syndrome (RTT) (1–4). Patients with RTT show normal early development until 6 to 18 months of age, when acquired language is lost, repetitive hand movements appear, and epilepsy develops in 60% to 80% of cases (2,4–6). *MECP2* dysfunction generates an opaque and complex cascade of structural and functional changes during development. How such changes produce features of the RTT clinical phenotype such as neuronal network hyperexcitability and seizures remains unclear.

An emerging tool for studying early human neuronal network development is in vitro multielectrode array (MEA) electrophysiological recordings (7–10). Neuronal cultures are plated over a grid of electrodes that measure the activity of neurons (8). Stereotypical patterns of spontaneous action potential firing first emerge in single neurons as they mature (7), and then neurons begin to fire action potentials in rapid succession followed by a period of relative quiescence (bursts)

(11). Over time, individual neuronal bursts synchronize to become network bursts (12–17), which are critical for the development of synapses (18,19). Activity patterns in RTT mutant networks, such as network burst duration and frequency, deviate from those observed in control networks, reflecting altered normal development (20).

Studies of animal models have reported that *MECP2* mutations disrupt synaptic function (1,21–23), and human stem cell-derived *MECP2* null excitatory neurons seem to form networks with reduced burst frequency (7). However, the same human *MECP2* null neurons, when isolated from the network, showed increased input resistance, suggesting hyperexcitable neurons (7). A puzzling question is how increased neuronal hyperexcitability can lead to decreased network bursts.

In the current study, we clarify these issues by recording the activity of human pluripotent stem cell-derived neuronal networks carrying *MECP2* mutations. We found that *MECP2* mutant networks exhibit a complex bursting pattern termed reverberating super burst (RSB), which consists of an initial

large-amplitude burst followed by lower-amplitude high-frequency minibursts. RSBs lead to an increase in the frequency of network bursts in *MECP2* null networks relative to controls. Finally, we explored mechanisms of RSB generation. We demonstrated that EGTA-AM (a slow-kinetic, membrane-permeable Ca^{2+} chelator) decreases RSB frequency, thereby rescuing *MECP2* null networks burst dynamics.

METHODS AND MATERIALS

The full methodology can be found in the [Supplement](#).

Cell Culture and Differentiation

Three human-derived stem cell lines were previously generated. Briefly, CLT L124W mutant induced pluripotent stem cell (iPSC) lines were derived from fibroblasts of a clinically diagnosed patient with RTT. WIBR3 was derived from an unaffected embryonic stem cell line, and PGPC14 was from an unaffected iPSC line. Isogenic pairs were generated via gene editing (WIBR3, PGPC14) or XCI assays (CLT). *NGN2* over-expression protocol differentiated PSC lines toward excitatory cortical neurons. Cell lines were examined for *MECP2* protein levels. For further information, refer to Mok *et al.* (7) and see the [Supplemental Materials and Methods 4.1](#).

MEA Plating and Recording

MEA plating was performed as described in Mok *et al.* (7). Briefly, 12-Well Cytoview plates (Axion Biosystems) containing 64 electrodes per well were prepared and seeded with day 8 *Ngn2* neurons. The following day, P1 mouse astrocytes were added, maintaining a 5:1 ratio of neurons to astrocytes. MEAs were recorded weekly on the Axion Maestro device using AxIS version 2.0 software and analyzed in Python. See the [Supplemental Materials and Methods 4.2](#).

Pharmacological Treatments

MEA plates were monitored, and pharmacological treatments began after RSBs were detected in culture. Before treatments, culture media was changed and allowed to stabilize, and baseline recordings were performed. Following baseline, 0.1% DMSO or 10 μM bicuculline was added to each well. Ten-minute posttreatment spontaneous activity was recorded. Culture media was changed 3 times to wash out treatment. EGTA-AM (25 μM) was always added as the final compound because it was observed that normal baseline spontaneous activity did not return even after washout. See the [Supplemental Materials and Methods 4.3](#).

Electrophysiological Analysis

All electrophysiological analysis was performed in Python. Briefly, RSB detection was performed using a 4-phase process: 1) signal conditioning, 2) burst detection loop, 3) reverberating network detection, and 4) reverberating super burst construction loop. Features were generated subsequently. See the [Supplemental Materials and Methods 4.4 through 4.10](#).

Statistical Analyses

Statistical tests were performed using Python (versions 3.9 and 3.11) and JASP (version 0.17.1). Comparisons between groups were conducted by 1-way analysis of variance, 2-way

repeated-measures analysis of variance and Kruskal-Wallis, Mann-Whitney, Wilcoxon matched paired signed rank, independent samples Student's *t*, and paired Student's *t* tests, with associated parametric and nonparametric post hoc tests where appropriate ($*p < .05$, $**p < .01$, $***p < .001$). Mono-exponential decay fit, Pearson correlation, linear regression, and random sample consensus (RANSAC) regression were used to identify best fits and correlations. All figures were created using Seaborn and Matplotlib. Schematics created with [BioRender.com](#).

RESULTS

A Hyperexcitability Phenotype in *MECP2* Null Single Neurons

Electrophysiological data recorded by Mok *et al.* from *MECP2* mutant excitatory neurons and neuronal networks, including their isogenic controls, were obtained from NDD-Ephys-dB (7) (Figure 1A) (see [Supplemental Materials and Methods 4.11](#)). In brief, Mok *et al.* generated excitatory neurons from 3 isogenic pairs of female pluripotent stem cell lines (WIBR3, PGPC14, and CLT) using the *Ngn2* protocol (Figure 1B) (7). The *MECP2* null pairs were derived by gene editing of the healthy WIBR3 human embryonic stem cell line or the PGPC14 healthy iPSC line. CLT iPSC lines were derived from an atypical patient with RTT with the milder phenotype of the preserved speech variant (heterozygous L124W missense mutation) and expressed only the mutant or the wild-type allele due to X-chromosome inactivation (Figure 1A, B).

We confirmed that WIBR3 *MECP2* null neurons show a lower rheobase than isogenic controls (Figure 1C–E). They also showed a progressive increase in firing rate that peaks and then declines with enhanced stimulus intensity (Figure 1D, E). On the other hand, isogenic controls showed higher rheobase but a sustained increase in firing frequency compared with *MECP2* null (Figure 1D, E). Spike rate adaptation, quantified as the slope of an exponential decay function fitted to the firing rate as a function of stimulation intensity, was stronger in *MECP2* null neurons than in controls (Figure 1F). These findings indicate that *MECP2* null single neurons, although more hyperexcitable, reach lower peak firing rates and undergo stronger spike rate adaptation than isogenic controls.

RSBs Emerge in *MECP2* Mutant Neuronal Networks

The seemingly contradictory finding from the earlier MEA phenotyping study was a decrease in network burst frequency and increased network burst duration in *MECP2* null networks relative to isogenic control networks (7). To probe this, we reanalyzed existing MEA data from the same isogenic pairs (7). Network activity was recorded for 5 minutes every week for 6 weeks (Figure S1). Here, we refer to the rate of action potentials across the different electrodes (i.e., channels) as network activity. As networks developed, network activity transitioned through various stages (described in the [Supplemental Results 1.1](#)). In week 6, wild-type control networks produced single-network bursts (Figure 2A). In contrast, in a subset of mutant networks, large-network events consisted of an initial single large-amplitude burst (initiation burst) followed by several high-frequency, lower-amplitude bursts (minibursts) (Figure 2B, C). The entire complex was termed an RSB due to a super burst

Hyperexcitability in Rett Syndrome Neuronal Networks

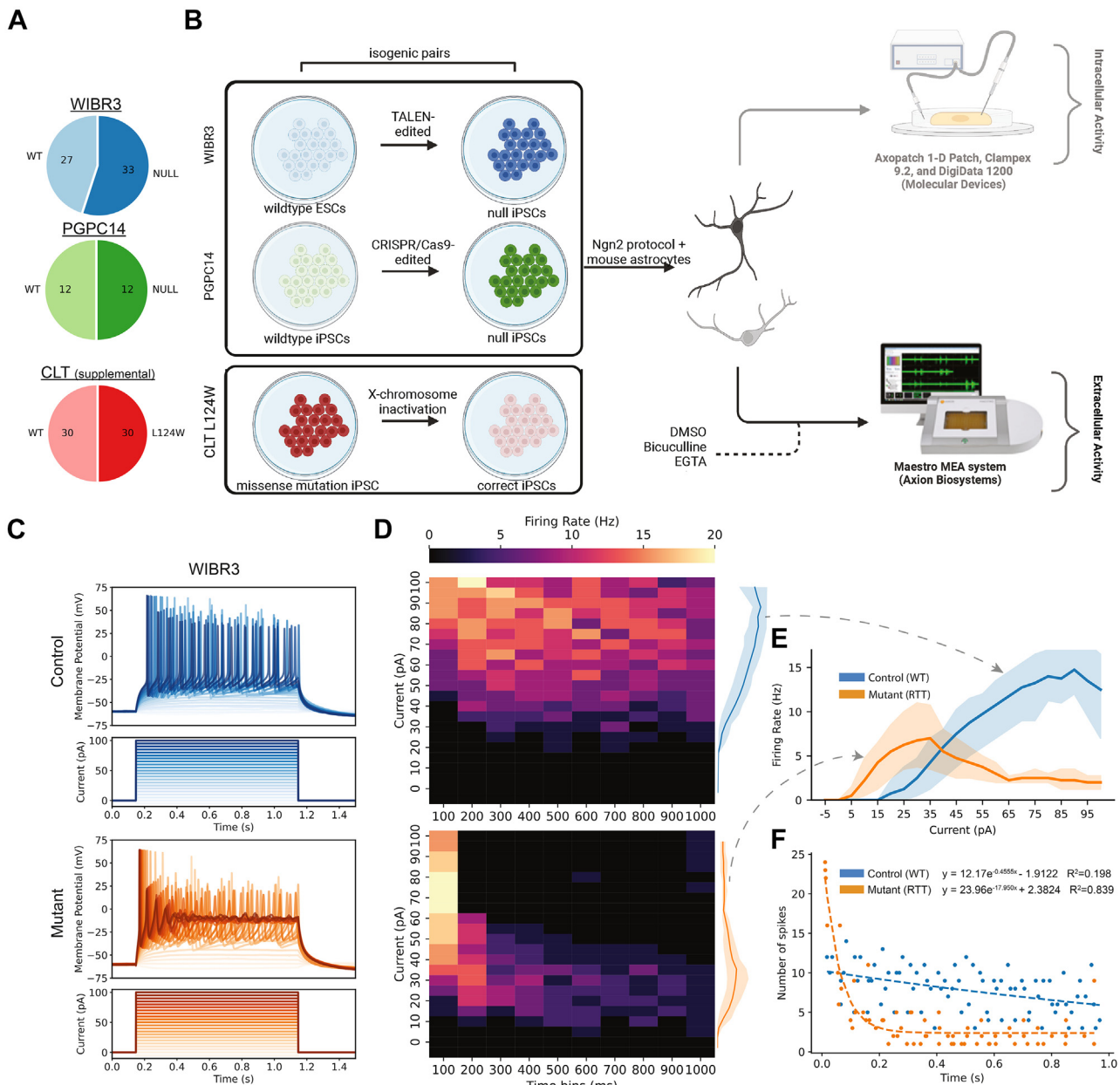


Figure 1. Study design and hyperexcitability in *MECP2* null single neurons. **(A)** Proportion of wild-type and *MECP2* mutant human stem cell lines used from Mok et al. (7), which can be found on NDD-Ephys-dB. **(B)** Schematic overview. Three female cell lines (WIBR3-unaffected embryonic stem cell; PGPC14-unaffected iPSC; CLT L124W-affected patient-derived iPSC) were used to generate 3 isogenic pairs, for a total of 6 lines. Each line was differentiated into excitatory neurons using a rapid single-step *Ngn2* differentiation protocol and plated overtop mouse astrocytes. Intracellular single-neuron activity was measured between weeks 4 and 5. Extracellular population activity was measured for 5 minutes weekly for 6 weeks. At week 5, pharmacological treatment with bicuculline and EGTA-AM was performed on WIBR3. CLT results can be found in the [Supplement](#). **(C)** Representative 1-second square pulse current clamp traces with 5-pA increments. **(D)** Firing rate heatmap of WIBR3 neurons with 100 ms time bins. **(E)** Input response curve of average WIBR3 intracellular activity. WIBR3 null single neurons exhibit lower rheobase, indicating hyperexcitability. **(F)** Exponential decay curve fit of the number of spikes per cell across sweeps over 1-second square pulse. WIBR3 null single neurons exhibit greater adaptation, indicated by steeper decay. CRISPR, clustered regularly interspaced short palindromic repeats; ESC, embryonic stem cell; iPSC, induced pluripotent stem cell; RTT, Rett syndrome; TALEN, transcription activator-like effector nuclease; WT, wild-type.

structure (17) that resembled acoustic reverberations (Figure 2B, C).

RSBs emerged at the network level, evident in the average instantaneous firing rate across all channels (Figure 2C,

bottom), but also appeared at a single-channel (i.e., electrode) (Figure 2C, top) and single-unit (i.e., single-neuron) level (Figure 2D). To demonstrate this, we built a spike density function to approximate the instantaneous firing rate (24).

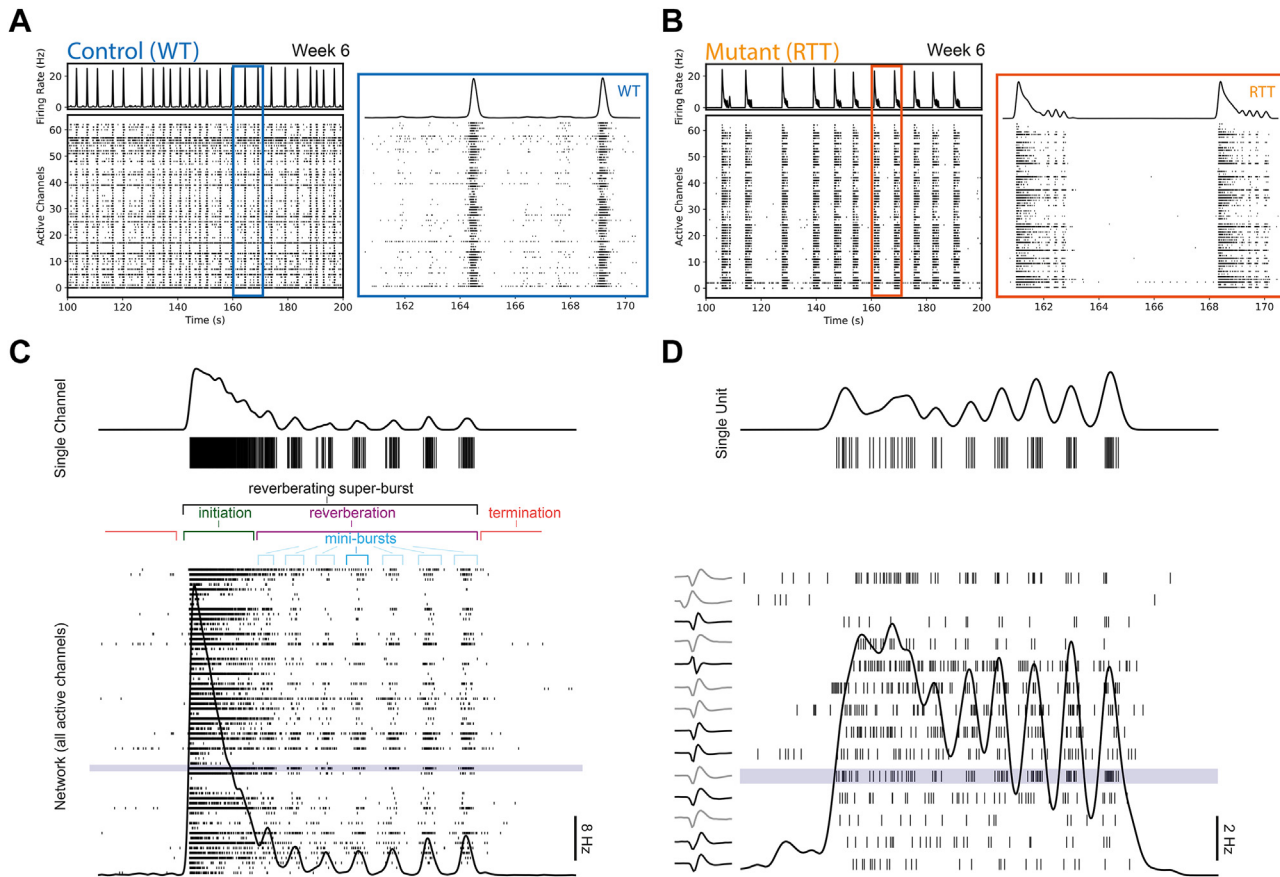


Figure 2. Reverberating super bursts emerge in *MECP2* mutant networks and occur at a single-unit, single-channel, and network level. **(A)** Representative raster plot and associated spike density function of WIBR3 wild-type networks (6 weeks postplating). **(B)** Representative raster plot and associated spike density function of WIBR3 null networks (6 weeks postplating). **(C)** (Bottom) Schematic of reverberating super burst containing an initiation network burst followed by reverberations of multiple minibursts. Black trace represents spike density function. (Top) Single-channel activity highlighted from a selected channel (blue). **(D)** (Bottom) Spike-sorted activity of the same reverberating super burst seen in **(C)**. (Top) Single-unit activity highlighted from a selected unit (blue). (Left) Extracellular action potential waveforms from each putative unit. RTT, Rett syndrome; WT, wild-type.

At the network level, the network averaged instantaneous firing rate demonstrated reverberating dynamics (Figure 2C). RSBs followed a stereotypical form (described in Figure 2C) containing an initiation network burst with a high-amplitude firing rate. RSBs ended with a period of quiescence that was longer than the interval between minibursts (Figure 2B, C). The initiation network burst was typically of longer duration (initiation burst median = 1.144 seconds, miniburst median = 0.359 seconds) and larger amplitude (initiation burst median = 25.668 Hz, miniburst median = 3.891 Hz) than the following minibursts.

To investigate whether RSBs were the product of multiunit (i.e., multiple neurons) activity or single-unit (i.e., single neuron) activity, we performed spike sorting using Plexon Offline Sorter in select reverberating wells (Figure 2D) (25). Spike sorting attempts to decouple single-unit activity from multiunit activity. Although most channels containing multiunit activity could not be sorted and were therefore discarded during quality control, in the sorted channels, RSBs persisted at the single-unit level (Figure 2D, top). However, RSB structure changed subtly, most notably in the amplitude of firing rate for the initiation burst

(Figure 2D, bottom). Thus, RSBs occurred in single units as well as in multiunits.

Inconsistent Handling and Detection of RSBs

Network burst-level features such as network burst frequency and network burst duration are commonly reported as phenotyping metrics in many disease modeling studies (8). In our *MECP2* mutant networks, RSBs exhibit various amplitude-frequency profiles (Figure S2). The consistent and accurate detection of network bursts by automated detection algorithms used in high-throughput analyses is essential for phenotypes to be reproducible. To examine how standard network burst detection algorithms handle RSBs, we reanalyzed the data using both fixed interspike interval (ISI) and adaptive ISI network burst detection algorithms (Figure 3A; see the Supplemental Results 1.2.1) (26–28). These approaches utilize an ISI threshold that can distinguish spiking activity as occurring within versus outside of bursts (26,28). Furthermore, we conducted a Welch power spectral density estimate previously used in Mok et al. (Figure 3B; see Supplemental Results 1.2.2) (7). These burst detection methods captured and

Hyperexcitability in Rett Syndrome Neuronal Networks

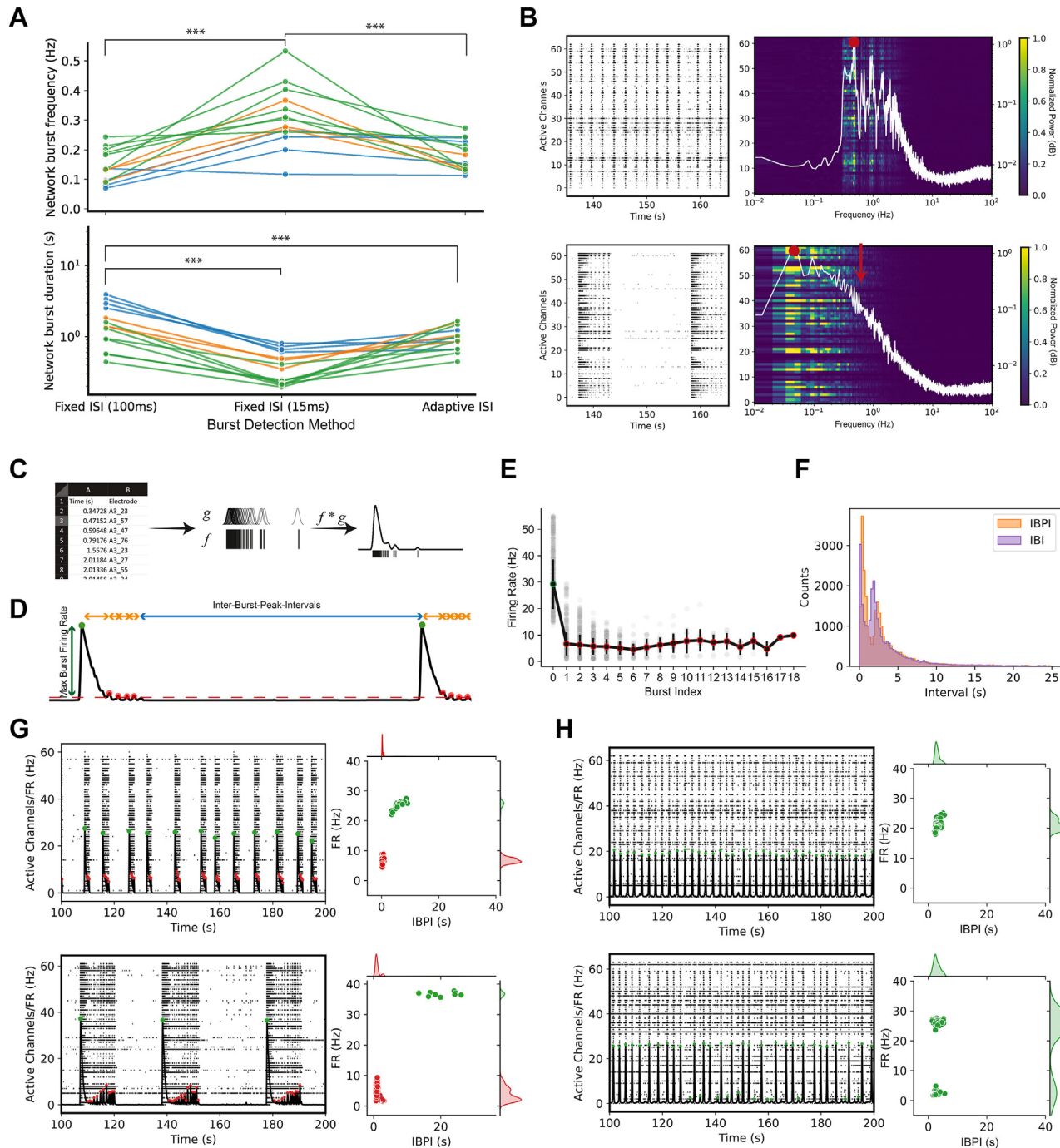


Figure 3. Inconsistent handling by standard burst detection algorithms and 2-feature detection of reverberating networks. **(A)** Comparison of network burst frequency (Top panel), and network burst duration (Bottom panel) by different ISI-based burst detection algorithms. Colors indicate replicates from the same plate. **(B)** Representative burst detection using power spectral density estimates [previously used in Mok *et al.* (7)]. Nonreverberating networks (Top panel) present with a sharp peak at the network burst frequency (0.493 Hz, red dot). Peaks at integer multiples of network burst frequency (i.e., fundamental frequency) represent harmonics (e.g., 0.98, 1.479, 1.97 Hz, etc.). Reverberating networks (Bottom panel) present with a broad peak at network burst frequency (red dot) but no peak at expected miniburst frequency (red arrow). White traces represent the average of the power spectral density for the network. The network and associated power spectral densities are representative examples of wild-type (top) or null (bottom) networks. **(C)** Calculation of spike density function by convolution of spike time with optimized Gaussian kernel. Spike density function represents an estimate of the instantaneous firing rate of the network. **(D)** Schematic of burst peak features. Bursts were identified by finding local peaks that exceed a minimum burst firing rate threshold (height) and change in firing rate (prominence). Dots represent detected burst peaks. **(E)** Burst peak firing rate (amplitude) relative to burst position (index) within a reverberating super burst. A burst position of 0 represents the initiation burst. Burst positions > 0 represent the minibursts. The initiation burst has a larger

described the same phenomenon in different, incomplete ways. We found that the experimenter's choice of burst detection algorithm and parameters significantly impacted where network burst boundaries were drawn within RSBs, which affected quantification of network phenotyping metrics in downstream analyses.

To develop an algorithm that reliably identifies RSBs, we first defined an RSB as an activity pattern containing various repetitive low-amplitude and high-frequency minibursts nested within a larger network event. Specifically, a large-amplitude network burst must precede the smaller amplitude minibursts (**Figure 3C–E**). The interburst intervals within the larger network event (typically of the minibursts) must be shorter than the interburst intervals between subsequent large network events, namely RSBs (**Figure 3D, F**). Then we utilized a network-level spike density function (**Figure 3C**) to detect local activity peaks that mapped onto network bursts (**Figure 3D–F**) and performed 2-dimensional clustering based on the burst firing rate and interburst peak interval (**Figure 3G, H; Figure S3**). Reverberating burst detection is further described in the [Supplemental Results 1.2.3](#) and the [Supplemental Materials and Methods 4.8](#). This approach allowed the categorization of networks as reverberating or nonreverberating and generated RSB-related features (see the [Supplemental Materials and Methods 4.9](#)).

MECP2 Null Networks Reverberate More Than Isogenic Control Networks

We categorized network activity into 3 groups based on the proportion of RSBs relative to the total number of detected bursts in the 3 isogenic *MECP2* mutant and control pairs (**Figure 4A**). These activity groups are 1) nonreverberating networks (<20% RSBs), 2) mixed reverberating networks (between 20% and 70% RSBs), and 3) reverberating networks (>70% RSBs). Comparisons of the distributions of reverberating networks between the isogenic pairs were performed and described by the network reverberation index (NRI) (**Figure 4B**; see [Supplemental Results 1.3.1](#)). A positive NRI, seen in WIBR3 and PGPC14, means that the mutant network contains more RSBs than isogenic controls (**Figure 4A, B**). A negative NRI indicates the opposite, and an NRI of 0 indicates that both contain the same number of RSBs. This was seen in the CLT pair, indicating no difference in the proportion of RSBs between isogenic pairs (**Figure S4**). This pattern is consistent with the milder atypical phenotype reported in this patient by Mok *et al.* (**7**).

Importantly, when considering minibursts contributing to the total number of network bursts, WIBR3 null networks showed increased network bursts relative to controls (log-transformed 2-way analysis of variance, $F_{3,167} = 3.888$, $p = .010$) (**Figure 4C**; see [Supplemental Results 1.3.2](#)). Thus, our results portray a different picture than Mok *et al.* (**7**). *MECP2* null neurons assemble into networks that produce more RSBs

than isogenic controls. The increase in RSBs causes an increase in network bursts and therefore network burst frequency, a trend that becomes clear during weeks 6 and 7 (**Figure 4C**). This result indicates that *MECP2* null networks are more excitable than isogenic controls, which corresponds to the more excitable single-neuron phenotypes reported in Mok *et al.* (**7**).

RSBs Bias the Calculation of Burst Metrics

To further investigate RSBs in *MECP2* mutants and controls, we focused on the WIBR3 networks where RSBs were most pronounced. We stratified WIBR3 networks into 4 groups: nonreverberating control (NR-WT), nonreverberating *MECP2* null (NR-NULL), reverberating control (R-WT), and reverberating null (R-NULL) networks (**Figure 5A**). These categories were based on the previously stated proportions (i.e., reverberating networks containing >70% RSBs, nonreverberating networks containing <20% RSBs, and excluding mixed reverberating networks).

In the following duration and frequency comparisons (detailed in the [Supplemental Results 1.4.1](#)), a network event refers to the entire RSB (initiation network burst and minibursts) in reverberating networks or discrete single-network bursts in nonreverberating networks. This was done to establish a link to the method used in Mok *et al.* that documented a decrease in network bursts in WIBR3 null mutants relative to controls (**Figure S5**) (**7**). In brief, network event duration (**Figure 5B**) was not significantly different between NR-WT and NR-NULL ($p_{\text{bonf}} = .788$), whereas R-NULL was significantly different from NR-NULL ($p_{\text{bonf}} < .001$) and NR-WT ($p_{\text{bonf}} < .001$). Network event duration was longer in R-NULL, which would be anticipated if such events are RSBs. All groups were significantly different from each other in network event frequency (NR-NULL × R-NULL interaction: $p_{\text{bonf}} < .05$; NR-NULL × NR-WT interaction: $p_{\text{bonf}} < .001$; R-NULL × NR-WT interaction: $p_{\text{bonf}} < .001$) (**Figure 5C**). Network event frequency was lowest in R-NULL networks (**Figure 5C**). This would also be anticipated in networks that show an increase in RSBs.

To explore the factors that influenced the changes in RSB duration and RSB frequency in reverberating networks, we examined the number of minibursts per RSB, RSB duration, and miniburst frequency between reverberating wild-type (R-WT) and R-NULL networks (**Figure 5D–G**; see [Supplemental Results 1.4.2](#)). Although RSBs were found in R-WT networks, their features differed from those in R-NULL networks, suggesting that *MECP2* deficiency exacerbates RSBs.

Most RSBs initiate with a longer-than-normal network burst. Therefore, we hypothesized that the length of the initiation burst may determine the probability that minibursts will follow. We compared the initiation burst duration in reverberating networks to nonreverberating single-network burst duration. Initiation burst duration was significantly longer in

amplitude than minibursts. Burst amplitude can be used to label bursts as either initiation bursts or minibursts. (**F**) Distribution of IBPI approximates the distribution of IBI. IBI is left-shifted relative to IBPI. (**G**) Examples of clustering results for reverberating networks. (**H**) Examples of clustering results for nonreverberating networks. Error bars (**E**) represent standard deviation. Red dots (**G,H**) represent labeled minibursts, whereas green dots represent initiation network bursts. Statistical significance was evaluated using 1-way analysis of variance. *** $p < .001$. FR, firing rate; IBI, interburst interval; IBPI, interburst peak interval; ISI, interspike interval.

reverberating networks than nonreverberating networks (Kruskal–Wallis, $H_3 = 4393.402$, $p < .001$) (Figure 5H). Finally, we found that longer initiation burst duration was associated with a faster miniburst frequency (RANSAC linear fit of week 6 inliers, $m = 0.4138$) (Figure 5I) and greater number of minibursts per RSB (RANSAC linear fit of week 6 inliers, $m = 0.1447$) (Figure 5J). These findings reflect the idiosyncratic developmental trajectory of *MECP2* null compared to isogenic controls.

RSBs Are Dependent on Asynchronous Ca^{2+} Release

We hypothesized that the mechanisms that are responsible for RSBs may operate at the level of the excitatory synapse. Therefore, by downregulating the amount of neurotransmitter release by partially blocking Ca^{2+} availability in the presynaptic terminal, RSBs may be rescued. First, we verified that our networks were composed of excitatory neurons by applying bicuculline (see *Supplemental Results 1.5*; Figure 6A–E). Then we applied EGTA-AM, which decreases Ca^{2+} and vesicular neurotransmitter release in the microdomain of single channels when they are not saturated (29). We reasoned that during minibursts, Ca^{2+} channels may not be saturated. In this case, we predicted that EGTA-AM could decrease miniburst frequency by binding to intracellular Ca^{2+}

and decreasing its availability at the presynaptic vesicular sensor. In contrast, Ca^{2+} channels may be saturated during typical high-amplitude bursts where intracellular Ca^{2+} is more abundant. Accordingly, we predicted that EGTA-AM should have a minimal effect on higher-amplitude network bursts.

EGTA-AM was applied to both NR-WT and R-NUL networks (Figure 6F). EGTA-AM eliminated the presence of RSBs in R-NUL networks (fold change = 0) and had no effect on RSBs in NR-WT networks (fold change = 1) (Figure 6F, G). Furthermore, EGTA-AM had a significant effect on network event frequency in R-NUL networks (Mann–Whitney, $p = .009$) (Figure 6H). As RSBs and therefore the minibursts were eliminated, EGTA-AM significantly decreased network event duration (Mann–Whitney, $p = .002$) (Figure 6I) in previously R-NUL networks (fold change = 0.082) but also had an effect in NR-WT networks (fold change = 0.537) (Figure 6I). We also compared DMSO vehicle-treated control network (DMSO-WT) (Figure 6J) features to EGTA-AM-treated null network (EGTA-NUL) (Figure 6K) and DMSO-treated null network (DMSO-NUL) (Figure 6L) features. We found no effect of DMSO, while the effect of EGTA-AM rescued network burst dynamics to similar levels of DMSO-WT (see *Supplemental Results 1.6*; Figure 6M–Q). In summary, EGTA-AM treatment of reverberating null networks reduced RSBs while preserving network

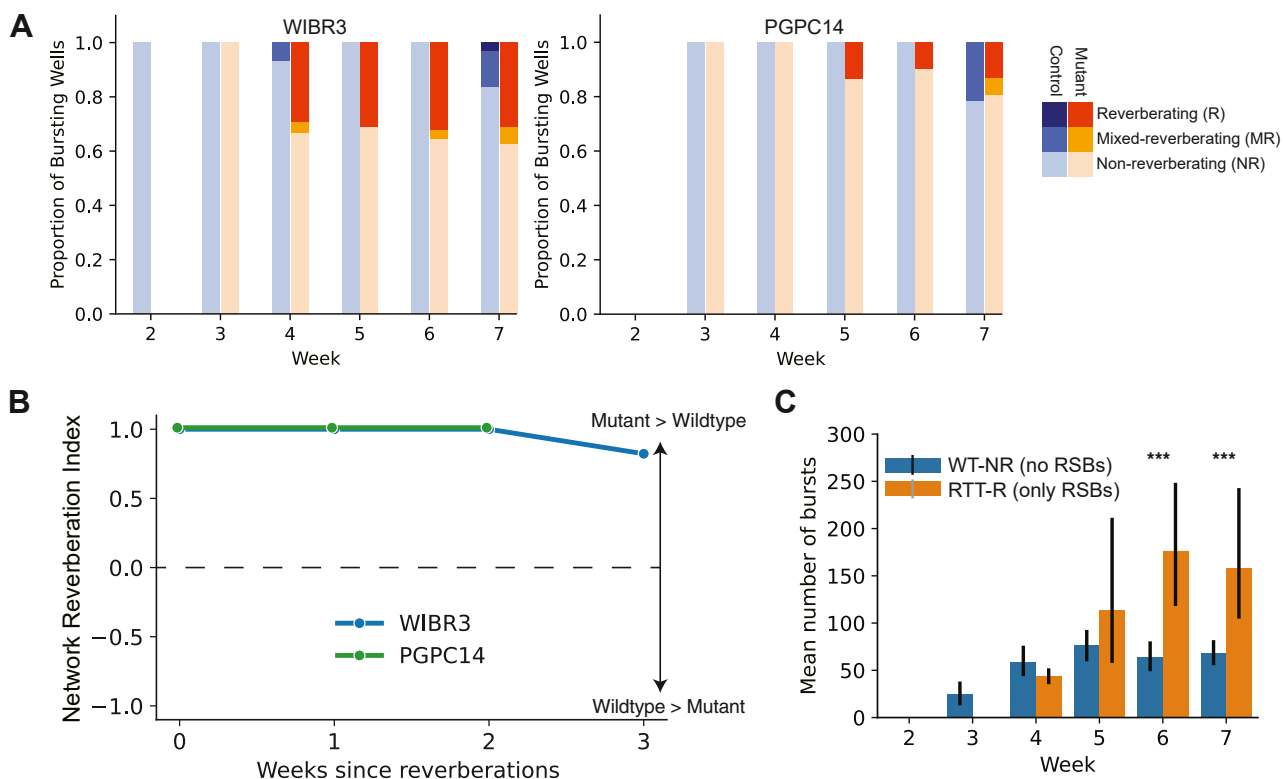


Figure 4. *MECP2* null networks reverberate more than isogenic controls and exhibit greater bursting activity, indicating hyperactivity. **(A)** Proportion of reverberating, mixed reverberating, and nonreverberating wells relative to the total number of bursting wells across development for each individual. **(B)** Network reverberation index, representing the plate-matched difference in proportion of reverberating networks for each individual. **(C)** Mean number of network bursts per recording for NR-WT and R-NUL networks. All bar plots use mean \pm 95% CIs. Statistical significance was evaluated using Kruskal–Wallis tests and 2-way analysis of variance. *** $p < .001$. RSB, reverberating super burst; RTT, Rett syndrome; WT, wild-type.

bursts with similar dynamics to nonreverberating wild-type networks.

EGTA-AM Decreases the Duration of the Initiation Network Burst

Because RSBs initiate with a longer-than-normal network burst, we asked whether EGTA-AM also reduces the duration

of the first network burst because it is possible that the rescue by EGTA-AM occurs at the expense of a reduction in the duration of the initial network burst. To test this hypothesis, we compared the burst duration of EGTA-treated null (EGTA-NULL) networks to DMSO-WT networks. DMSO treatment had no significant effect on the duration of discrete network bursts in nonreverberating control (DMSO-WT) networks or the initiation burst duration in reverberating null (DMSO-NULL)

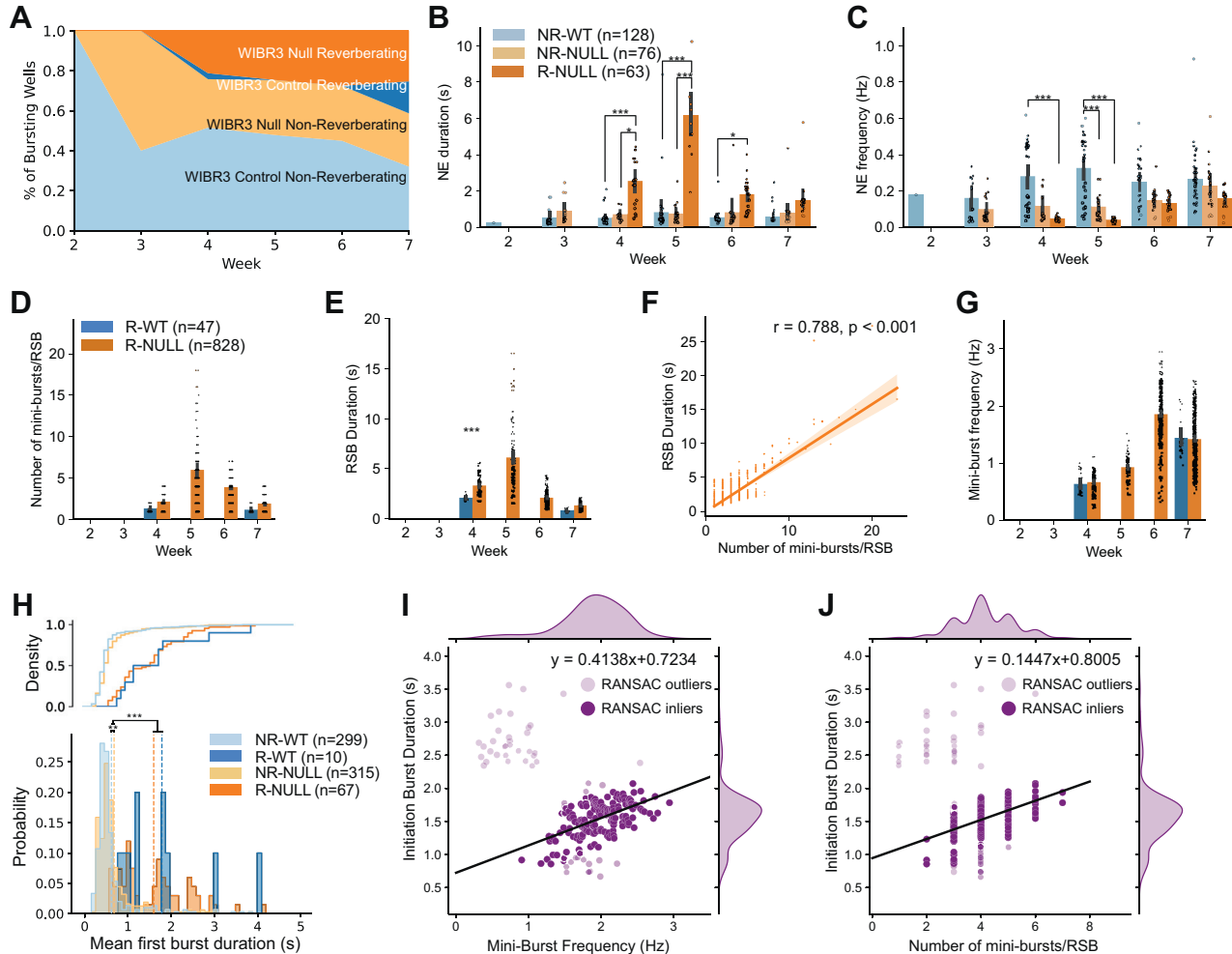


Figure 5. RSBs alter network bursting metrics. **(A)** Wild-type and MECP2 null WIBR3 networks were stratified as either nonreverberating or reverberating. **(B, C)** Quantification of **(B)** network event duration and **(C)** network event frequency between nonreverberating control networks (NR-WT), nonreverberating mutant networks (NR-NULL), and reverberating mutant networks (R-NULL). Network event refers to the entire RSBs (initiation network burst and minibursts) in reverberating networks or discrete single-network bursts in nonreverberating networks. **(D)** Quantification of the number of minibursts per RSB of reverberating WIBR3 WT (R-WT) and WIBR3 null (R-NULL) networks. **(E)** Quantification of RSB duration of reverberating R-WT and R-NULL networks. **(F)** Linear regression of number of minibursts per RSB and RSB duration in R-NULL networks suggests the long network burst duration is associated with an increased number of minibursts that were unaccounted for. **(G)** Quantification of reverberating miniburst frequency of R-WT and R-NULL networks. **(H)** Distribution of initiation burst duration in reverberating (R-WT and R-NULL) networks and discrete single-network burst duration of nonreverberating (NR-WT and NR-NULL) networks. **(I)** RANSAC regression of miniburst frequency and initiation burst duration in week 6 R-NULL networks suggests that a longer initiation burst duration is associated with increased reverberating miniburst frequency. Lighter colored points indicate RANSAC outliers. Darker colored points indicate RANSAC inliers. Linear fit performed on RANSAC inliers. See RANSAC Regression under [Supplemental Materials and Methods 4.10](#). **(J)** RANSAC regression of number of minibursts per RSB and initiation burst duration in week 6 R-NULL networks suggests longer initiation burst duration is associated with increased number of minibursts that follow. Lighter colored points indicate RANSAC outliers. Darker colored points indicate RANSAC inliers. Linear fit performed on RANSAC inliers. See RANSAC regression under [Supplemental Materials and Methods 4.10](#). All bar plots use mean \pm 95% CIs. Statistical significance was evaluated using 2-way analysis of variance, Kruskal-Wallis test, linear regression, and RANSAC regression. * $p < .05$, ** $p < .01$, *** $p < .001$. NE, network event; NR, nonreverberating; R, reverberating; RANSAC, random sample consensus; RSB, reverberating super bursts; WT, wild-type.

Hyperexcitability in Rett Syndrome Neuronal Networks

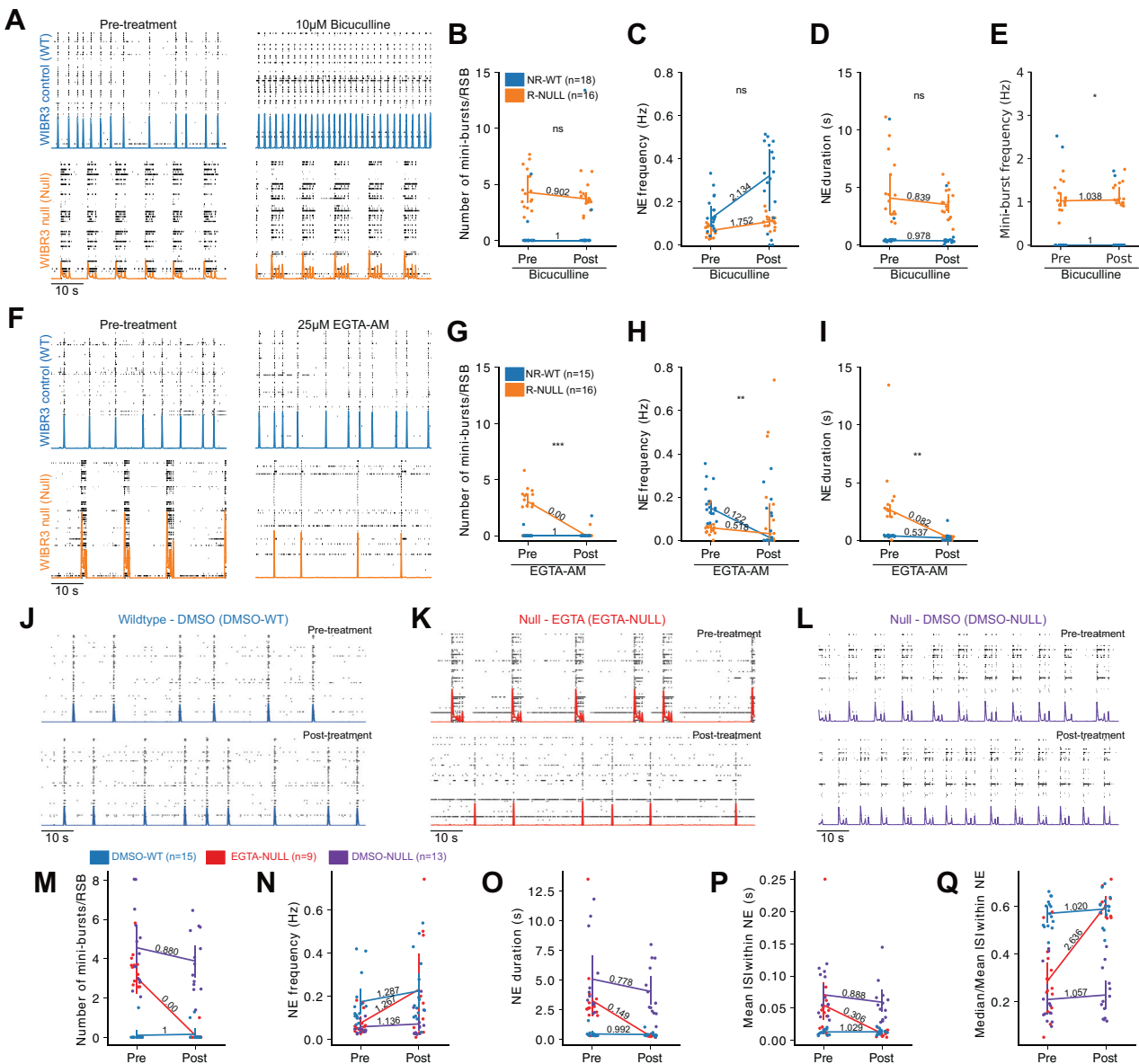


Figure 6. Pharmacological treatment of EGTA-AM and not bicuculline eliminates RSBs and rescues network bursting phenotype. **(A)** Representative raster plot of WIBR3 WT and null networks before and after bicuculline treatment. WIBR3 WT networks did not reverberate (NR-WT) whereas WIBR3 null networks did (R-NULL). **(B-E)** Quantification of **(B)** number of minibursts per RSB, **(C)** network event duration, **(D)** network event frequency, and **(E)** miniburst frequency in pre- and postbicuculline-treated WIBR3 networks. **(F)** Representative raster plot of WIBR3 NR-WT and R-NULL networks before and after EGTA-AM treatment. **(G-I)** Quantification of **(G)** number of minibursts per RSB, **(H)** network event duration, and **(I)** network event frequency in pre- and post-EGTA-AM-treated WIBR3 networks. **(J)** Representative raster plot of WIBR3 NR-WT networks before and after DMSO treatment. **(K)** Representative raster plot of WIBR3 R-NULL networks before and after EGTA treatment. **(L)** Representative raster plot of WIBR3 R-NULL networks before and after DMSO treatment. **(M-Q)** Quantification of **(M)** number of minibursts per RSB, **(N)** network event frequency, **(O)** network event duration, **(P)** mean interspike interval within network event, and **(Q)** median/mean ISI within network event in pre- and post-DMSO-treated WT networks (DMSO-WT), pre- and post-EGTA-AM-treated null (EGTA-NULL) networks, and pre- and post-DMSO-treated null (DMSO-NULL) networks. Point plots use mean **(B-E, G-I)** and median **(M-Q)** \pm 95% CIs. Fold change label indicated over respective line plot. Statistical significance was evaluated using Mann-Whitney test, independent samples Student's *t* test, Kruskal-Wallis and Dunn's post hoc test. **p* < .05, ***p* < .01, ****p* < .001. ISI, interspike interval; NE, network event; ns, not significant; RSB, reverberating super burst; WT, wild-type.

networks (Kruskal-Wallis, Dunn's post hoc, $p_{bonf} = 1.000$ and $p_{bonf} = 1.000$, respectively) (Figure 7A). In contrast, EGTA-AM reduced the duration of the initiation burst in previously reverberating null (EGTA-NULL) networks (Kruskal-Wallis,

Dunn's post hoc, $p_{bonf} < 0.001$) (Figure 7B-D). Additional comparisons are reported in the *Supplemental Results 1.7*. These results suggest that the long initiation burst duration may trigger the minibursts. Moreover, they suggest that the

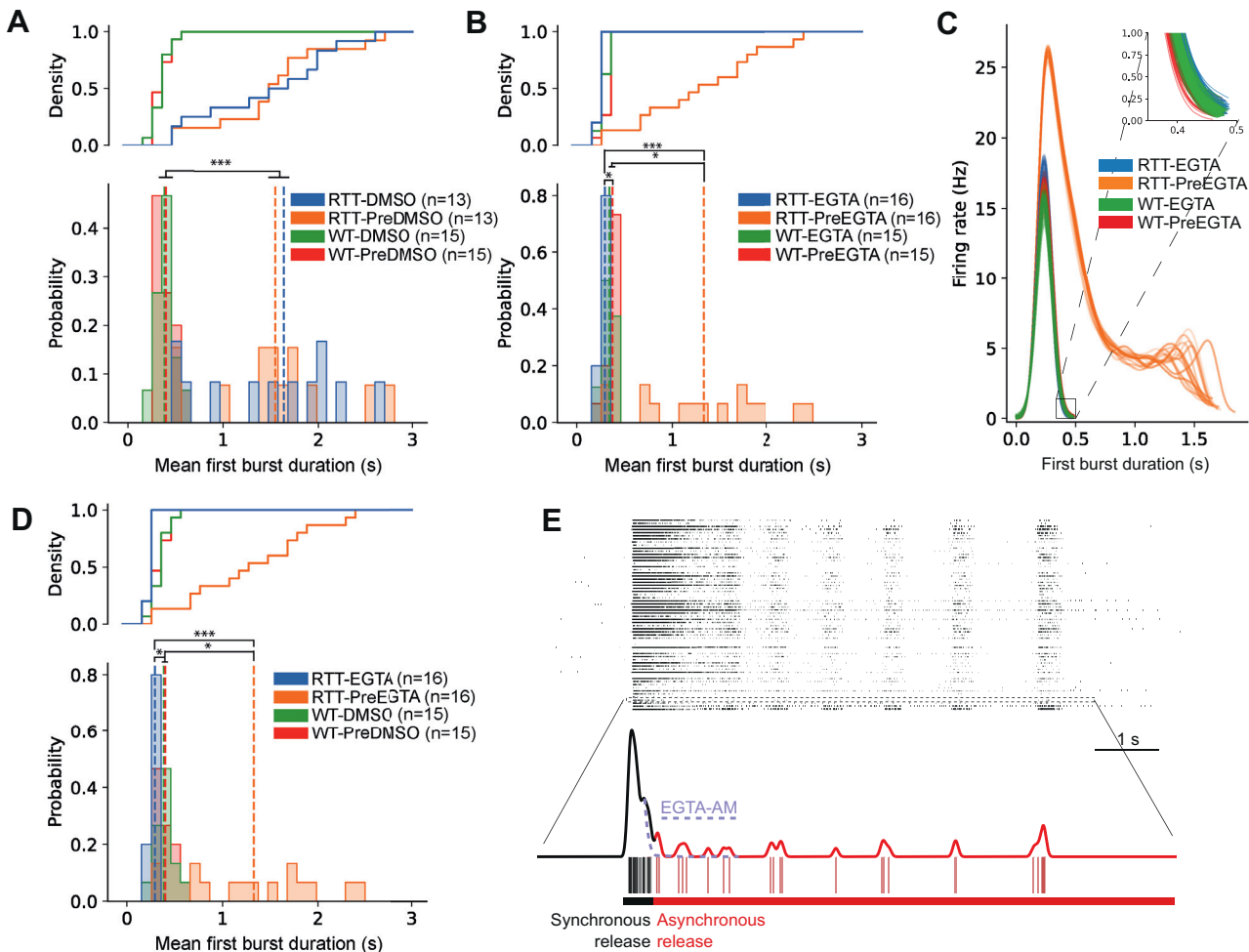


Figure 7. EGTA-AM reduces the duration of the initiation network burst in reverberating super bursts. **(A, B, D)** Cumulative distribution function and associated histogram of mean burst duration of nonreverberating wild-type networks compared with the duration of the initiation network burst of reverberating *MECP2* null networks (NULL). Dashed lines represent the mean burst duration per group. **(A)** Distribution of burst duration in response to DMSO treatment to both null (DMSO-NULL) and WT (DMSO-WT). **(B)** Distribution of burst duration in response to EGTA treatment to both null (EGTA-NULL) and WT (EGTA-WT). **(C)** Overlaid truncated spike density function of each first burst duration for preEGTA-WT, preEGTA-NULL, EGTA-WT, and EGTA-NULL. Representative networks were used. **(D)** Distribution of burst duration in response to DMSO treatment in WT (DMSO-WT) networks and EGTA treatment in null (EGTA-NULL) networks. **(E)** Hypothesized mechanism for elongated initiation burst in reverberating super bursts. The dashed line represents the effect of EGTA-AM treatment on initiation burst duration. Statistical significance was evaluated using 1-way analysis of variance, Kruskal-Wallis test, and Dunn's post hoc comparisons. $p < .05$, $***p < .001$. RTT, Rett syndrome; WT, wild-type.

hyperexcitable reverberating event can be rescued by reducing the availability of intracellular Ca^{2+} and subsequent asynchronous neurotransmitter release (Figure 7E).

DISCUSSION

We investigated the development of *MECP2* mutant *Ngn2* human PSC-derived excitatory networks using electrophysiological methods and compared them to isogenic controls. We report the following findings: 1) *MECP2* null neurons showed increased excitability and spike frequency adaptation in patch-clamp recordings; 2) *MECP2* null networks showed an increased proportion of RSB consisting of a large initial network burst followed by several smaller-amplitude, high-

frequency minibursts that overall produce greater network burst frequencies in MEA recordings; and 3) administration of EGTA-AM (a slow-kinetic membrane-permeable Ca^{2+} chelator) decreases RSBs rescuing the bursting network phenotype.

Single-Neuron and Network Excitability in *MECP2* Null Neurons

We corroborated our previous report (7) and showed that *MECP2* null neurons have increased excitability, which accounts for the decrease in rheobase to elicit action potentials and increased adaptation and for the fast decay in firing rate during sustained stimulation. A contradictory finding was that

despite this hyperexcitability in single neurons, analysis using standard burst detection algorithms suggested network hypoexcitability (described in the [Supplemental Discussion 3.1.1](#)) (7). We showed that this was due to the classification of complex RSBs as single-network events. Using our algorithm to classify the minibursts contained in RSBs as independent events, *MECP2* null networks demonstrated an increased total number of network bursts, consistent with the hyperexcitability phenotype seen in single neurons. Thus, hyperexcitable *MECP2* null neurons led to a hyperexcitable bursting phenotype in neuronal networks.

Another contradictory finding was the report of reduced mean firing rate in *MECP2* null networks, which indicates hypoactivity (described in the [Supplemental Discussion 3.1.2](#)) (7). This can be reconciled by strong spike frequency adaptation experienced in *MECP2* null neurons. Two properties, hyperexcitability and strong adaptation, may make *MECP2* null neurons have a strong propensity for firing minibursts following a long initiation burst within an RSB. Because minibursts are composed of fewer spikes, this results in increased network bursts but a decreased mean firing rate relative to control networks over the entire recording. Because bursts are more likely to influence postsynaptic integration and excitation more than isolated spikes, we interpret these results as a hyperexcitability phenotype in *MECP2* nulls relative to isogenic controls.

Some nonreverberating mutant networks showed no differences in network burst duration relative to nonreverberating isogenic control networks. This indicates variability in hyperexcitability that is possibly caused by compensatory mechanisms that can restore normal network development even in the absence of *MECP2*. Furthermore, some isogenic control networks also produced RSBs, suggesting that RSBs are not unique to *MECP2* mutant networks and may be more ubiquitous in MEA studies than previously reported (30–35). It may be that RSBs are a normal part of network activity development but emerge earlier and more often and persist longer in *MECP2* null networks.

Mechanisms of RSB Generation

The proposed mechanisms of rapid fluctuations in neuronal activity that produce reverberations can be grouped into: 1) abnormalities in the excitation/inhibition balance (36), 2) abnormalities in synaptic calcium dynamics (37–40), and 3) an interplay between the two (41). Contrary to studies that have implicated excitation-inhibition balance in RSBs (detailed in the [Supplemental Discussion 3.2.1](#)), our *MECP2* null networks, lacking inhibitory interneurons, still exhibited RSBs. This indicates that these bursts are not solely dependent on excitation-inhibition synaptic interplay. In contrast, EGTA-AM, which impacts slow-kinetic synaptic calcium dynamics, effectively eliminated RSBs and rescued burst metrics in reverberating networks. EGTA-AM may create the possibility of rescuing network hyperexcitability phenotypes during the early stages of neurodevelopment. Further investigation is needed due to the important role of Ca^{2+} in neuronal excitability during development.

One possible explanation for the observed RSBs involves elevated presynaptic Ca^{2+} , which promotes asynchronous

neurotransmitter release (42). Asynchronous release occurs when Ca^{2+} levels remain elevated even after the initial stimulus has ended, typically after moderate-to-high-frequency stimulation [detailed in [Supplemental Discussion 3.2.2](#) and (39,42)]. The decrease in rheobase in our *MECP2* null neurons may also have contributed to the recruitment of voltage-sensitive Ca^{2+} channels in the presynaptic terminal and triggered asynchronous neurotransmitter release (43). Reverberating networks also had a prolonged initiation burst duration compared with non-reverberating networks, which EGTA-AM reduced. This finding suggests that longer initiation burst duration may produce elevated presynaptic Ca^{2+} levels, triggering reverberating minibursts (detailed in [Supplemental Discussion 3.2.2.1](#)). It is likely that *MECP2* null networks exist in a genetically predisposed hyperexcitable state such that physiologically relevant stimuli are more likely to trigger a network reverberation. RSBs can induce long-term potentiation in synapses and trigger mechanisms of synaptic plasticity (42,44–46) and may serve as a predisposing factor for the development of disorders of hyperexcitability such as epilepsy, which is common in patients with RTT and has been shown to have numerous etiologies (40,47–50).

The ability of excitatory networks to generate RSBs associated with their connectivity level has also been linked to asynchronous neurotransmitter release (38,39). Because bursting patterns similar to RSBs have previously been reported in healthy, developing neuronal networks, it may be that RSBs represent a normal transition during network development as neurons functionally integrate more strongly with each other [detailed in [Supplemental Discussion 3.2.3](#) and (17)]. Therefore, hypoconnected *MECP2* null networks may persist in a bursting regime that is dominated by RSBs, unable to transition into a mature network state. In contrast, hyper-connected networks in other neurodevelopmental disorders may resolve RSBs by establishing mature network states more quickly than controls and may require more frequent MEA recordings to reliably capture RSB activity. The CLT phenotype is discussed in the [Supplemental Discussion 3.3](#).

The rescue of the hyperexcitable phenotype by EGTA-AM suggests that Ca^{2+} dynamics are critical for the emergence of RSBs. Our findings demonstrate that *MECP2* null neurons exhibit hyperexcitability that can be rescued pharmacologically. If the RSB mechanism persists into childhood, it may predispose patients with RTT with *MECP2* null mutations to develop seizures and provide insight into possible Ca^{2+} -mediated pharmacological interventions for epilepsy.

ACKNOWLEDGMENTS AND DISCLOSURES

This work was supported by Simons Foundation Autism Research Initiative (Grant No. 514918 [to JE and JM-T]), Canadian Institutes of Health Research ERARE Team Grant (Grant No. ERT161303 [to JE]), Canadian Institutes of Health Research Project Grant (Grant No. PJT168905 [to JE]), Canadian Institutes of Health Research Foundation Grant (Grant No. FDN-154336 [to MWS]), an award from the John Evans Leadership Fund & Ontario Research Fund (to JE), an award from the Canada Research Chair in Stem Cell Models of Childhood Disease (to JE), an award from the Beta Sigma Phi International Endowment Fund (to JE), and an award from BrainsCAN at Western University through the Canada First Research Excellence Fund (to KSP and JM-T). Trainee support was provided by a Natural Sciences and Engineering Research Council Postgraduate Scholarship–Doctoral Scholarship (to KSP) and an Autism Speaks Predoctoral Award and David Stephen Cant Scholarship in Stem Cell Research (to FPM).

We thank Dr. Indra R. Bishnoi for her review and editing of the manuscript. We thank Rebecca Mok for providing data to NDD-Ephys-dB.

KSP, FPM, MK, JE, and JM-T were responsible for conceptualization; KSP, FPM, WW, JE, and JM-T were responsible for methodology; KSP was responsible for formal analysis; FPM, WW, and WZ were responsible for investigation; FPM and WW were responsible for resources; KSP, FPM, and MK were responsible for data curation; KSP, FPM, MK, JE, and JM-T were responsible for writing the original draft of the article; KSP, FPM, MK, WZ, MWS, JE, and JM-T were responsible for reviewing and editing the manuscript; KSP was responsible for visualization; JE and JM-T were responsible for supervision; KSP, FPM, MWS, JE, and JM-T were responsible for funding acquisition. All authors revised and approved the paper.

The data can be found on NDD-Ephys-dB. NDD-Ephys-dB is a resource for *in vitro* electrophysiological datasets explicitly related to human neurodevelopmental disorders, including Rett Syndrome (described in the [Supplemental Materials and Methods 4.11](#)).

A previous version of this article was published as a preprint on bioRxiv: <https://doi.org/10.1101/2023.09.12.557388>.

The authors report no biomedical financial interests or potential conflicts of interest.

ARTICLE INFORMATION

From the Graduate Program in Neuroscience, Schulich School of Medicine & Dentistry, Western University, London, Ontario, Canada (KSP, JM-T); Robarts Research Institute, Western University, London, Ontario, Canada (KSP, MK, JM-T); Department of Molecular Genetics, University of Toronto, Toronto, Ontario, Canada (FPM, JE); Developmental & Stem Cell Biology, The Hospital for Sick Children, Toronto, Ontario, Canada (FPM, WW, JE); Neuroscience & Mental Health, The Hospital for Sick Children, Toronto, Ontario, Canada (WZ, MWS); Department of Physiology, University of Toronto, Toronto, Ontario, Canada (MWS); Western Institute for Neuroscience, Western University, London, Ontario, Canada (JM-T); Department of Physiology and Pharmacology, and Psychiatry, Schulich School of Medicine & Dentistry, Western University, London, Ontario, Canada (JM-T); and Department of Psychiatry, Schulich School of Medicine & Dentistry, Western University, London, Ontario, Canada (JM-T).

KSP and FPM contributed equally to this work.

Address correspondence to James Ellis, Ph.D., at jellis@sickkids.ca, or Julio Martinez-Trujillo, M.D., Ph.D., at julio.martinez@robarts.ca.

Received Oct 18, 2023; revised Dec 20, 2023; accepted Jan 14, 2024.

Supplementary material cited in this article is available online at <https://doi.org/10.1016/j.bpsgos.2024.100290>.

REFERENCES

- Banerjee A, Castro J, Sur M (2012): Rett syndrome: Genes, synapses, circuits, and therapeutics. *Front Psychiatry* 3:34.
- Amir RE, Van den Veyver IB, Wan M, Tran CQ, Francke U, Zoghbi HY (1999): Rett syndrome is caused by mutations in X-linked MECP2, encoding methyl-CpG-binding protein 2. *Nat Genet* 23:185–188.
- Ip JPK, Mellios N, Sur M (2018): Rett syndrome: Insights into genetic, molecular and circuit mechanisms. *Nat Rev Neurosci* 19:368–382.
- Vashi N, Justice MJ (2019): Treating Rett syndrome: From mouse models to human therapies. *Mamm Genome* 30:90–110.
- Cardoza B, Clarke A, Wilcox J, Gibbon F, Smith PEM, Archer H, et al. (2011): Epilepsy in Rett syndrome: Association between phenotype and genotype, and implications for practice. *Seizure* 20:646–649.
- Opero FF, Mazza R, Pastorino GMG, Verrotti A, Coppola G (2019): Epilepsy and genetic in Rett syndrome: A review. *Brain Behav* 9: e01250.
- Mok RSF, Zhang W, Sheikh TI, Pradeepan K, Fernandes IR, DeJong LC, et al. (2022): Wide spectrum of neuronal and network phenotypes in human stem cell-derived excitatory neurons with Rett syndrome-associated MECP2 mutations. *Transl Psychiatry* 12:450.
- McCready FP, Gordillo-Sampedro S, Pradeepan K, Martinez-Trujillo J, Ellis J (2022): Multielectrode arrays for functional phenotyping of neurons from induced pluripotent stem cell models of neurodevelopmental disorders. *Biology* 11:316.
- Deneault E, Faheem M, White SH, Rodrigues DC, Sun S, Wei W, et al. (2019): CNTN5^{-/-} or EHMT2^{-/-} human iPSC-derived neurons from individuals with autism develop hyperactive neuronal networks. *eLife* 8:e40092.
- Nagesappa S, Carromeu C, Trujillo CA, Mesci P, Espuny-Camacho I, Pasciutto E, et al. (2016): Altered neuronal network and rescue in a human MECP2 duplication model. *Mol Psychiatry* 21:178–188.
- Zeldnerust F, Wadman WJ, Englitz B (2018): Neural coding with bursts-current state and future perspectives. *Front Comput Neurosci* 12:48.
- Cabrera-Garcia D, Warm D, de la Fuente P, Fernández-Sánchez MT, Novelli A, Villanueva-Balsera JM (2021): Early prediction of developing spontaneous activity in cultured neuronal networks. *Sci Rep* 11:20407.
- Kamioka H, Maeda E, Jimbo Y, Robinson HPC, Kawana A (1996): Spontaneous periodic synchronized bursting during formation of mature patterns of connections in cortical cultures. *Neurosci Lett* 206:109–112.
- Opitz T, De Lima AD, Voigt T (2002): Spontaneous development of synchronous oscillatory activity during maturation of cortical networks *in vitro*. *J Neurophysiol* 88:2196–2206.
- Tozzi A, Zare M, Benasich AA (2016): New perspectives on spontaneous brain activity: Dynamic networks and energy matter. *Front Hum Neurosci* 10:247.
- Ruthazer ES, Akerman CJ, Cline HT (2003): Control of axon branch dynamics by correlated activity *in vivo*. *Science* 301:66–70.
- Wagenaar DA, Pine J, Potter SM (2006): An extremely rich repertoire of bursting patterns during the development of cortical cultures. *BMC Neurosci* 7:11.
- Kerschensteiner D (2014): Spontaneous network activity and synaptic development. *Neuroscientist* 20:272–290.
- Belykh I, de Lange E, Hasler M (2005): Synchronization of bursting neurons: What matters in the network topology. *Phys Rev Lett* 94: 188101.
- Luhmann HJ, Sining A, Yang JW, Reyes-Puerta V, Stüttgen MC, Kirischuk S, Kilb W (2016): Spontaneous neuronal activity in developing neocortical networks: From single cells to large-scale interactions [cited Nov 24 2022]. *Front Neural Circuits* 10:40.
- Boggio EM, Lonetti G, Pizzorusso T, Giustetto M (2010): Synaptic determinants of Rett syndrome. *Front Synaptic Neurosci* 2:28.
- Della Sala G, Pizzorusso T (2014): Synaptic plasticity and signaling in Rett syndrome. *Dev Neurobiol* 74:178–196.
- Fukuda T, Itoh M, Ichikawa T, Washiyama K, Goto Y (2005): Delayed maturation of neuronal architecture and synaptogenesis in cerebral cortex of MeCP2-deficient mice. *J Neuropathol Exp Neurol* 64:537–544.
- Shimazaki H, Shinomoto S (2010): Kernel bandwidth optimization in spike rate estimation. *J Comput Neurosci* 29:171–182.
- Corrigan BW, Gulli RA, Doucet G, Roussy M, Luna R, Pradeepan KS, et al. (2022): Distinct neural codes in primate hippocampus and lateral prefrontal cortex during associative learning in virtual environments. *Neuron* 110:2155–2169.e4.
- Cotterill E, Charlesworth P, Thomas CW, Paulsen O, Eglen SJ (2016): A comparison of computational methods for detecting bursts in neuronal spike trains and their application to human stem cell-derived neuronal networks. *J Neurophysiol* 116:306–321.
- Pasquale V, Martinoia S, Chiappalone M (2010): A self-adapting approach for the detection of bursts and network bursts in neuronal cultures. *J Comput Neurosci* 29:213–229.
- Bakkum DJ, Radivojevic M, Frey U, Franke F, Hierlemann A, Takahashi H (2013): Parameters for burst detection. *Front Comput Neurosci* 7:193.
- Nakamura Y (2019): EGTA Can Inhibit vesicular release in the nano-domain of single Ca²⁺ channels. *Front Synaptic Neurosci* 11:26.
- Droge MH, Gross GW, Hightower MH, Czisny LE (1986): Multielectrode analysis of coordinated, multisite, rhythmic bursting in cultured CNS monolayer networks. *J Neurosci* 6:1583–1592.
- Pimashkin A, Kastalskiy I, Simonov A, Koryagina E, Mukhina I, Kazantsev V (2011): Spiking signatures of spontaneous activity bursts in hippocampal cultures. *Front Comput Neurosci* 5:46.
- Heikkilä TJ, Ylä-Outinen L, Tanskanen JMA, Lappalainen RS, Skottman H, Suuronen R, et al. (2009): Human embryonic stem

- cell-derived neuronal cells form spontaneously active neuronal networks in vitro. *Exp Neurol* 218:109–116.
- 33. Matsuda N, Odawara A, Katoh H, Okuyama N, Yokoi R, Suzuki I (2018): Detection of synchronized burst firing in cultured human induced pluripotent stem cell-derived neurons using a 4-step method. *Biochem Biophys Res Commun* 497:612–618.
 - 34. Odawara A, Katoh H, Matsuda N, Suzuki I (2016): Physiological maturation and drug responses of human induced pluripotent stem cell-derived cortical neuronal networks in long-term culture. *Sci Rep* 6: 26181.
 - 35. Iida S, Shimba K, Sakai K, Kotani K, Jimbo Y (2018): Synchronous firing patterns of induced pluripotent stem cell-derived cortical neurons depend on the network structure consisting of excitatory and inhibitory neurons. *Biochem Biophys Res Commun* 501:152–157.
 - 36. Trujillo CA, Gao R, Negraes PD, Gu J, Buchanan J, Preissl S, et al. (2019): Complex oscillatory waves emerging from cortical organoids model early human brain network development. *Cell Stem Cell* 25:558–569.e7.
 - 37. Huang CH, Huang YT, Chen CC, Chan CK (2017): Propagation and synchronization of reverberatory bursts in developing cultured networks. *J Comput Neurosci* 42:177–185.
 - 38. Volman V, Gerkin RC, Lau PM, Ben-Jacob E, Bi GQ (2007): Calcium and synaptic dynamics underlying reverberatory activity in neuronal networks. *Phys Biol* 4:91–103.
 - 39. Dao Duc K, Lee CY, Parutto P, Cohen D, Segal M, Rouach N, Holcman D (2015): Bursting reverberation as a multiscale neuronal network process driven by synaptic depression-facilitation. *PLoS One* 10:e0124694.
 - 40. Holcman D, Tsodyks M (2006): The emergence of up and down states in cortical networks. *PLoS Comput Biol* 2:e23.
 - 41. Lau PM, Bi GQ (2005): Synaptic mechanisms of persistent reverberatory activity in neuronal networks. *Proc Natl Acad Sci USA* 102:10333–10338.
 - 42. Kaeser PS, Regehr WG (2014): Molecular mechanisms for synchronous, asynchronous, and spontaneous neurotransmitter release. *Annu Rev Physiol* 76:333–363.
 - 43. Catterall WA (2011): Voltage-gated calcium channels. *Cold Spring Harb Perspect Biol* 3:a003947.
 - 44. Iremonger KJ, Bains JS (2007): Integration of asynchronously released quanta prolongs the postsynaptic spike window. *J Neurosci* 27:6684–6691.
 - 45. Lu T, Trussell LO (2000): Inhibitory transmission mediated by asynchronous transmitter release. *Neuron* 26:683–694.
 - 46. Hjelmsstad GO (2006): Interactions between asynchronous release and short-term plasticity in the nucleus accumbens slice. *J Neurophysiol* 95:2020–2023.
 - 47. McCormick DA, Shu Y, Hasenstaub A, Sanchez-Vives M, Badoual M, Bal T (2003): Persistent cortical activity: Mechanisms of generation and effects on neuronal excitability. *Cereb Cortex* 13:1219–1231.
 - 48. Staley K (2015): Molecular mechanisms of epilepsy. *Nat Neurosci* 18:367–372.
 - 49. Blumenfeld H (2005): Cellular and network mechanisms of spike-wave seizures. *Epilepsia* 46(suppl 9):21–33.
 - 50. Sanchez-Vives MV, McCormick DA (2000): Cellular and network mechanisms of rhythmic recurrent activity in neocortex. *Nat Neurosci* 3:1027–1034.